

Calibration of Laminar Flow Meters for Process Gases

John D. Wright^a, Thiago Cobu^b, Robert F. Berg^a, and Michael R. Moldover^a

^aNational Institute of Standards and Technology, Gaithersburg, MD, USA
Tel: 301-975-5937, Fax: 301-258-9201, E-mail: john.wright@nist.gov, rberg@nist.gov,
Michael.moldover@nist.gov

^bPresent address, Instituto de Pesquisas Tecnológicas, Sao Paulo, Brazil
Tel: 55 11 3767 4604, Fax: 55 11 3766 3572, E-mail: thiagoc@ipt.br

Abstract:

We calibrated three models of commercially-manufactured, laminar flow meters (LFMs) at four pressures (100 kPa, 200 kPa, 300 kPa, and 400 kPa) with five gases (N₂, Ar, He, CO₂, and SF₆) over a 10:1 flow range using NIST's primary flow standards as references. We combined three items: (1) the calibration data acquired with N₂, (2) gas-property data from NIST's database REFPROP 9.0, and (3) a physical model for each LFM that accounts for the effects of viscosity, entrance and exit effects, gas expansion, gas non-ideality, and slip. This combination predicted the calibrations for the flow of Ar, He, CO₂, and SF₆ with a maximum error of 0.8 % for Reynolds numbers $Re < 500$. Under these conditions, the present LFM model allows prediction of calibration results for other gases with approximately 3 times more accuracy than conventional approaches that plot the flow coefficient as a function of the viscosity coefficient or Re . We represented the calibration data for SF₆ in the range $500 < Re < 2000$ by adding an empirical quadratic function to the model for one of the LFMs.

1. Introduction

The users and manufacturers of flow meters for process gases often calibrate meters with one gas and use them to measure the flow of other gases. Below, we show that this can be done in the range $Re < 500$ with a maximum error of only 0.8 % for three different, commercially-manufactured, laminar flow meters (LFMs) by calibrating each meter with nitrogen. We obtained these accurate results for the test gases Ar, He, CO₂, and SF₆ by combining the nitrogen-determined calibration coefficients with gas-property data from NIST's database REFPROP 9.0 [1]. For each meter and each gas, the data span the pressure range 100 kPa to 400 kPa and a 10:1 flow range.

The starting point for our LFM models is one of the best-understood flow meters for gases near 100 kPa, a long, straight capillary with plenums at each end. In a first approximation, the flow through such a capillary is deduced from the Hagen-Poiseuille equation using the measured temperature, the viscosity of the gas, and measurements of the stagnation pressure in each plenum. When higher accuracy is desired, correction terms with theoretically estimated coefficients are added to the Hagen-Poiseuille equation to account for the effects of kinetic

energy, gas expansion, gas non-ideality, slip, and several, less-important phenomena [2]. The flow paths in commercially-manufactured LFM's are not long, straight capillaries. Therefore, the correction terms in this work have coefficients that depend on the geometry of each LFM. As shown in [3], these coefficients can be estimated from the geometry of each meter. Here, we obtained errors less than 0.8 % in the range $Re < 500$ by fitting two of the coefficients and the hydraulic diameter D_h to nitrogen-based calibration data for each LFM.

When we extrapolated the nitrogen-based calibration above $Re = 500$, the errors in the test gas flows grew with Re , reaching 0.9 % to 7.5 % (depending upon the specific LFM). This is not surprising because at $Re = 1800$, the largest correction term reaches 5 % to 43 % of the Hagen-Poiseuille term. For two LFM's, we obtained acceptable calibrations in the extended range $0 < Re < 1800$ by fitting the same coefficients to the calibration data for all five gases rather than nitrogen alone. For the third LFM in the extended range, we could fit the flow data for all five test gases with the same coefficients plus a second-order function of Re . Thus, $Re = 500$ is a practical limit for extrapolating nitrogen calibrations to other gases for the LFM's studied, the same value identified by Feng et. al [4].

2. Physical Model for the Laminar Flow Meters

The simplest model for a laminar flow meter is the Hagen-Poiseuille (H-P) equation

$$\dot{m} = \frac{\pi \rho r^4 (P_1 - P_2)}{8 \eta L}, \quad (1)$$

which relates the mass flow of an incompressible fluid through a capillary of circular cross section to the density ρ and dynamic viscosity η of the fluid, the capillary radius r and length L , and the pressure drop $P_1 - P_2$ along the capillary.

The assumptions of the Hagen-Poiseuille (H-P) equation are [5]:

1. the flow has negligible kinetic energy,
2. the flow is laminar and steady,
3. the capillary is straight and has a uniform, circular cross section,
4. the fluid is incompressible and its density is constant,
5. the fluid is Newtonian,
6. the temperature of the fluid is constant and viscous heating is negligible,
7. there is no slip at the wall of the capillary.

The first assumption is invalid when the upstream and downstream pressures are measured at taps located in large chambers (plenums) upstream and downstream from the capillary, in which the flow velocity is much smaller than in the capillary. Pressure drops associated with development of the laminar flow profile at the entrance and jetting at the exit are called entrance and exit effects or kinetic energy effects. Conventional presentations of LFM calibration data account for laminar flow viscous effects (the H-P equation) and for kinetic energy effects [6] by plotting the flow coefficient FC as a function of the viscosity coefficient VC with the definitions:

$$FC \equiv \frac{L^3 \rho (P_2 - P_1)}{\eta \dot{m}} \quad \text{and} \quad VC \equiv \frac{L^2 \rho (P_2 - P_1)}{\eta^2}. \quad (2)$$

In prior work, Wright showed how to choose length scales so that $VC = (4L^3/r^3)Re$ for a circular capillary [7]. Therefore, we will replace conventional plots of FC vs VC with plots of FC vs Re , to facilitate comparing the conventional approach to our more complete physical model.

The third H-P assumption is invalid for two of the present flow meters, which have noncircular cross sections. Fortunately, hydrodynamic equations have been derived for a variety of cross sections; see, for example, Shah and London [8] or White [9]. The fourth assumption of incompressibility is invalid for gases. However, combining Eq. (1) with the ideal gas law for density at the average pressure $(P_1 + P_2)/2$ gives an expression that is simple and accurate to within a few percent for most LFMs:

$$\dot{m}_0 = \frac{\pi \mathcal{M} r^4 (P_1^2 - P_2^2)}{16 \eta(T, 0) L R T}, \quad (3)$$

Here R is the universal gas constant, T is the temperature, \mathcal{M} is the molar mass, and $\eta(T, 0)$ is the gas viscosity evaluated at temperature T in the limit of zero pressure.*

Further improving the accuracy requires corrections for the following five effects:

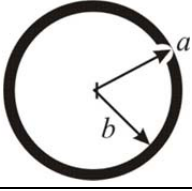
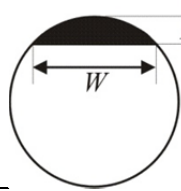
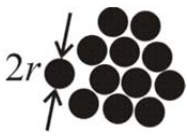
1. Density dependence of the gas viscosity and departures from the ideal gas law (g_{virial} term in Eqs. (4) and (6)).
2. Slip at the capillary wall, which increases the flow. This effect is proportional to the Knudsen number Kn , which is the gas mean free path divided by a length that characterizes the capillary cross section (K_{slip} term). See Eq. (11) for the definition of Kn .
3. The increase of kinetic energy near the capillary entrance, which decreases the flow. A correction with the same functional form arises where the flow exits the capillary and enters the downstream plenum ($K_{\text{ent}} + K_{\text{exit}}$ terms). The decreased flow is due to the pressure drop associated with Bernoulli's principle.
4. Gas expansion along the capillary, which increases the kinetic energy and decreases the flow (K_{exp} term).
5. The transverse temperature distribution in the fluid due to the imperfect cancellation of cooling due to gas expansion and viscous heating due to shear (g_{therm} term).

In [2] and [10], Berg used the results of previous researchers [5, 11, 12] to develop a combination of corrections for these five effects. Equation 4 summarizes the result for the mass flow through a single, long, straight, circular tube [2]:

$$\dot{m} = \dot{m}_0 \left[1 + g_{\text{virial}}(P_1, P_2) + 4K_{\text{slip}}Kn + \frac{K_{\text{ent}} + K_{\text{exit}}}{16} \frac{r}{L} Re + \left(\frac{K_{\text{exp}}}{8} + \frac{g_{\text{therm}}}{16} \right) \frac{r}{L} Re \ln \left(\frac{P_2}{P_1} \right) \right], \quad (4)$$

* All pressures used herein are absolute.

Table 1. Properties of three laminar flow meters: cross section geometry (not to scale), full scale flow, dimensions, and the parameters of the generalized LFM model (Eqs. (6)-(12)). For each meter, D_h was fitted to the nitrogen flow data. Then, more accurate calibrations were obtained by fitting the dimensionless coefficients ($K_{ent} + K_{exit}$), K_{exp} , and, in the case of the circular segment, also fitting a quadratic function of Re .

Flow meter	Annular	Circular segment	Circular ($n = 12$)
Geometry			
Full Scale (sccm)*	1000	100	1000
Length of LFE (mm)	60	60	75
Fitted D_h (mm)	$2(a - b) = 0.0696$	$H = 0.0803$	$2r = 0.427$
Additional length (mm)	$a = 3.95$	$W = 1.6$	
L/D_h	860	674	175
α	6	4	4
β	$(a - b)/(12L)$	$H/(24L)$	$r/(16L)$
γ	$(a - b)/(20L)$	$9H/(140L)$	$r/(16L)$
δ	$\pi a(a - b)^3/6$	$WH^3/96$	$\pi r^4/16$
p_w	$2\pi(a + b)$	$2W$	$2\pi r$
Estimated ($K_{ent} + K_{exit}$)	-0.90	-1.00	-1.14
($K_{ent} + K_{exit}$) fitted to all gases	-0.55	-1.17	-1.32
Estimated K_{exp}	1	1	1
K_{exp} fitted to all gases	1	0.55	0.4

*sccm = standard cubic centimeter per minute at 101.325 kPa and 0 °C.

The commercially manufactured LFMs studied in this work are not long, straight tubes with a circular cross section. Table 1 characterizes the three LFMs used in this study. The circular LFM is a bundle of 12 short tubes with no flow passage in the interstitial spaces. The annular LFM has a solid cylinder of radius b centered inside a hollow cylinder of a slightly larger radius a . The circular segment LFM has a solid cylinder of diameter D (not identified on figure in Table 1) with a small flat ground along its length inside a hollow cylinder of the same diameter. The resulting cross section is a shallow circular segment whose width W and maximum height H are related, in the limit of small W/D , by*

$$H = \frac{W^2}{4D}. \quad (5)$$

We describe the flow through the commercially manufactured LFMs with annular, circular and circular-segment cross sections using the same functional form as Eq. (4) but with different geometric parameters. To emphasize this, we generalize Eq. (4) to

* In our prior publication [3], Eq. (5) was incorrectly written: $H=W^2/(2D)$.

$$\dot{m} = \dot{m}_0 \left[1 + g_{\text{virial}}(P_1, P_2) + \alpha K_{\text{slip}} Kn + \beta (K_{\text{ent}} + K_{\text{exit}}) Re + \gamma (2K_{\text{exp}} + g_{\text{therm}}) Re \ln \left(\frac{P_2}{P_1} \right) \right], \quad (6)$$

where the geometrical parameters α , β , and γ for the three LFM are listed in Table 1 (see references [2] and [3] for derivations). Similarly, the Hagen-Poiseuille mass flow for a circular cross section is generalized as

$$\dot{m}_0 \equiv \delta \frac{\mathcal{M}(P_1^2 - P_2^2)}{\eta(T, 0) LRT}, \quad (7)$$

where the geometrical parameter δ is also listed in Table 1.

The five corrections in Eq. (6) depend on the Reynolds number Re , the Knudsen number Kn , the function g_{virial} , which corrects for the density dependence of the gas viscosity and departures from the ideal gas law, and the function g_{therm} , which depends upon the gas and the LFM shape. The function g_{therm} accounts for viscous heating and for the cooling of the gas as it expands along the capillary.

For all three LFM geometries, the length scale used in the Reynolds number is the hydraulic diameter,

$$D_H = \frac{4A}{p_w}, \quad (8)$$

where A and p_w are respectively the area and “wetted perimeter” of the cross section. The Reynolds number for an LFM is

$$Re = \frac{4\dot{m}}{p_w \eta(T, \bar{P})}, \quad (9)$$

where $\eta(T, \bar{P})$ is the viscosity evaluated at the pressure averaged along the length of the capillary [10]:

$$\bar{P} = \frac{1}{L} \int_0^L P(x) dx \cong \frac{2}{3} \frac{(P_1^3 - P_2^3)}{(P_1^2 - P_2^2)}. \quad (10)$$

Values of the geometric parameters p_w and D_h for each cross section are listed in Table 1. Note that by substituting Eqs. (7) and (9) into Eq. (6) and rearranging, an explicit expression for mass flow can be written. This rearranged equation can be used to calculate the flow through a calibrated LFM.

Equation (6) for the mass flow and Eq. (9) for the Reynolds number are for a single flow path. The circular LFM shown in Table 1 has 12 parallel tubes; therefore, the model flow must be multiplied by $n = 12$ for this LFM.

The Knudsen number is defined as

$$Kn \equiv \frac{\lambda_{1/2}}{D_h / 2}, \quad (11)$$

where

$$\lambda_{1/2} \equiv \left(\frac{2RT}{\mathcal{M}} \right)^{1/2} \frac{\eta(T, P_{1/2})}{P_{1/2}}, \quad (12)$$

is the mean free path evaluated at $P_{1/2} \equiv (P_1 + P_2) / 2$.

The expressions for the annular and circular segment models are approximations that are valid in the respective limits $H \ll W$ and $(a - b) \ll a$. For the annular model, the exact solution for δ is [8, 9]

$$\delta = \frac{\pi}{8} \left[a^4 - b^4 - \frac{(a^2 - b^2)^2}{\ln(a/b)} \right], \quad (13)$$

which simplifies to the approximate expression listed in Table 1 that shows that the flow depends on the cube of the gap between the cylinders. The derivation of the circular segment model is in reference [3].

For some LFM geometries, the values of K_{slip} , K_{ent} , K_{exit} , K_{exp} and g_{therm} can be calculated from analytic theory or computational fluid dynamics. Occasionally, prior researchers have measured them experimentally. Calculating K_{slip} and g_{therm} involves few and safe assumptions, and it is difficult to justify departures from their theoretical values ($K_{\text{slip}}=1$). This is not the case for $(K_{\text{ent}} + K_{\text{exit}})$ and K_{exp} because their values depend on details of the three commercial LFMs that we do not know, such as the size and shape of the plenums. Even if we knew the geometries, theoretical calculations would be difficult. Hence, we used theory to choose the functional form of the LFM corrections (Eq. 6) and fitted the equation to calibration data to determine the values for $(K_{\text{ent}} + K_{\text{exit}})$ and K_{exp} . To the extent that our model, Eq. (6), is successful, the values of $(K_{\text{ent}} + K_{\text{exit}})$ and K_{exp} determined from flow measurements with one gas (e.g. nitrogen) will work for other gases.

It is possible to apply Eq. (6) to LFMs with different geometries. To do so, one would use expressions for α , β , γ , and δ analogous to those in Table 1, If such expressions were not available, one would fit the parameters α , β , γ , and δ to nitrogen calibration data. For example, the entrance correction, which is $K_{\text{ent}}r/(16L)$ for the circular cross section, would be described simply as $(K_{\text{ent}} + K_{\text{exit}}) r/L$, where r is a characteristic transverse dimension, L is the LFM length, and $(K_{\text{ent}} + K_{\text{exit}})$ could be much different from 1.

3. Description of the LFM Calibrations

A pressure regulator and mass flow controller were used to set the flow of gas through the laminar flow meter as shown in Figure 1. A back-pressure regulator or a throttling valve was used to maintain a nominal pressure at the exit of the LFM despite increases in the upstream pressure. With this equipment, each LFM was tested at flows of 10 %, 25 %, 50 %, 75 %, and 100 % of full scale, and the nominal pressures at the LFM exit were 100 kPa, 200, kPa, 300 kPa, and 400 kPa. This arrangement gave at least 20 combinations of flow and pressure for each flow meter and each gas. The gases used were nitrogen, argon, helium, carbon dioxide, and sulfur hexafluoride. The data plotted herein are averages of 10 or more individual flow measurements made at each combination.

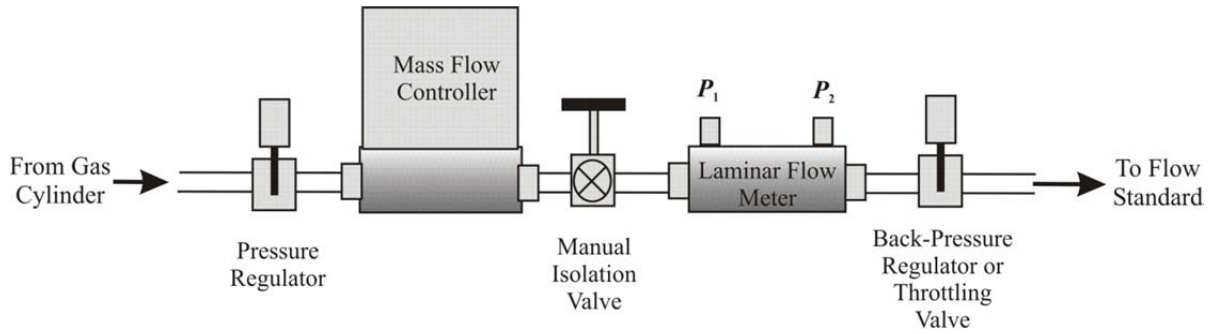


Figure 1. Schematic of the test arrangement to calibrate the laminar flow meters against the *PVTt* and *RoR* flow standards.

For the circular segment LFM and the annular LFM, P_1 and P_2 were measured with two absolute pressure sensors with a full scale of 550 kPa. The differential pressures ranged from 2 kPa to 63 kPa. Periodic taring of the two sensors kept the expanded* uncertainty of the differential pressures within 10 Pa, i.e. 0.5 % of the minimum differential pressure.

For the circular LFM, P_1 was measured with a 1400 kPa full scale sensor (0.04 % uncertainty). The differential pressure $P_1 - P_2$ ranged from 0.1 kPa to 2.6 kPa, and it was measured with a 1 kPa or a 10 kPa full scale sensor with uncertainty of 2 Pa. The LFM gas temperature (0.08 % uncertainty) was measured by placing sensors in good contact with the LFM body.

Three flow standards were used to calibrate the LFMs and to evaluate the LFM physical model:

1) *PVTt*: The 34 L Pressure-Volume-Temperature and time (*PVTt*) standard determined the mass of gas accumulated in a collection tank over a measured period of time. Details about this standard and its expanded uncertainty of 0.025 % can be found in reference [13].

2) *Rate-of-Rise*: At 10 sccm, it takes 57 h to make a single *PVTt* flow measurement that fills the 34 L collection tank from vacuum to 100 kPa. The Rate-of-Rise technique allows the same tank and instrumentation to be used more efficiently. This method acquires time-stamped pressure and temperature values for the gas in the collection tank while the tank is filling. The pressure and temperature are used to calculate the density of gas. The mass of gas at each time step is obtained by multiplying the calculated density by the collection volume, V . At each time t_i , the derivative of the accumulated mass with respect to time is the mass flow, i.e.:

$$\dot{m} = \frac{d}{dt} [V \rho(P, T)] \cong V \left[\frac{\rho(P_{i+1}, T_{i+1}) - \rho(P_i, T_i)}{t_{i+1} - t_i} \right], \quad (14)$$

For the present measurements, this technique has an expanded uncertainty of 0.054 %.

3) *Dynamic Gravimetric*: A commercial dynamic gravimetric flow standard was used to measure the mass of a pressurized gas cylinder as a function of time while discharging through the LFM. Its expanded uncertainty is 0.1 % [14].

The three flow standards agreed with each other within 0.05 %.

* Uncertainties herein are expanded, $k = 2$, with a 95 % confidence level unless otherwise stated.

4. Results and Discussion

Figures 2, 4, and 6 summarize our results by plotting the ratio of the flow calculated by a particular LFM model to the reference flow measured with the reference flow standards. For each LFM, the hydraulic diameter D_h was fitted to a single set of nitrogen flow data and used consistently throughout the analysis, i.e. the value of D_h that minimized the difference between the model and experimental data for nitrogen at low Re was determined. Each plot includes the flow and pressure combinations for all five gases. The four panels for each LFM in Figures 2, 4 and 6 compare the following sequence of LFM models:

- (A) The conventionally used flow coefficient (FC), defined in Eq. (2), which was fitted by a second-order polynomial in Re .
- (B) Eq. (6) with values of K_{slip} , $(K_{ent} + K_{exit})$, K_{exp} and g_{therm} determined analytically, computationally, or experimentally, based on prior research (“estimated K values”).
- (C) Eq. (6) with $(K_{ent} + K_{exit})$ and K_{exp} values fitted to the nitrogen flow data (“ K values fitted to N_2 ”).
- (D) Eq. (6) with $(K_{ent} + K_{exit})$ and K_{exp} values fitted to the flow data for all five gas species (“ K values fitted to all gases”).

No fitting was necessary for K_{slip} because the theoretical value of 1 worked well. For plots (C) and (D), the values of $(K_{ent} + K_{exit})$ and K_{exp} were fitted by iterating the following two steps:

- 1) Adjust $(K_{ent} + K_{exit})$ until the slope of model / standard flow versus Re plot (like Figure 2) is approximately zero.
- 2) Adjust K_{exp} to minimize dispersion of the model / standard values at the highest Re values (where expansion corrections are largest).

In the case of the circular cross section LFM, differences up to 2 % remained for large Reynolds numbers even after fitting Eq. (6) to all five gases. For that LFM, we multiplied Eq. (6) by an *ad hoc* second-order function of Re . (See also the discussion near the end of this section.)

Figure 2 shows the results for the annular LFM. In panel (A), a second-order fit of FC versus Re gives a flow ratio within 2 % of the standard; however, this conventional approach does not correct for slip flow effects evident in the helium data by vertical separation of data taken at different pressures. Panel (B) of Fig. 2 demonstrates the benefit of the slip corrections. In panel (C), $(K_{ent} + K_{exit})$ and K_{exp} were fitted to the N_2 flow data; however, when this model is extrapolated to the SF_6 data at large values of Re , the flow ratios have errors of 1 %. Panel (D) shows the results when $(K_{ent} + K_{exit})$ and K_{exp} are fitted to the flow data for all five gases: all flow ratios are within 0.4 % of the flow standard.

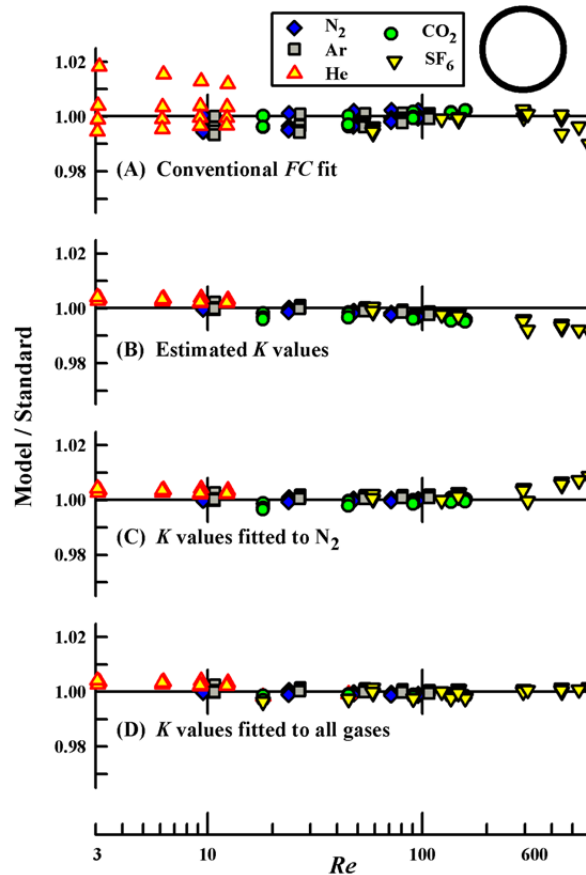


Figure 2. Flow ratio versus Reynolds number for the annular LFM for various model versions.

The annular LFM has the lowest maximum Re (600) and the largest aspect ratio ($1/\beta = 20640$) of the three LFMs tested; hence the limitations of Eq. (6) are not severely tested. The largest correction for any test condition for this LFM is the virial correction for SF_6 at 400 kPa, and it was only 4.7 % of the H-P flow.

For the annular LFM, Figure 3 displays the relative importance of the five correction terms in Eq. (6) for two representative cases: helium at 100 kPa and nitrogen at 400 kPa. These plots were obtained by using the K values fitted to all gases to calculate the individual terms in Eq. (6). The large aspect ratio yields small entrance and exit corrections ($< 0.3\%$). However, the relatively small transverse length ($a - b$) leads to a large Knudsen number, particularly for low pressure helium, and it gives slip corrections as large as 3.5 %. For a fixed exit pressure, the slip correction decreases with increasing flow or Re because the average pressure increases, which shortens the mean free path.

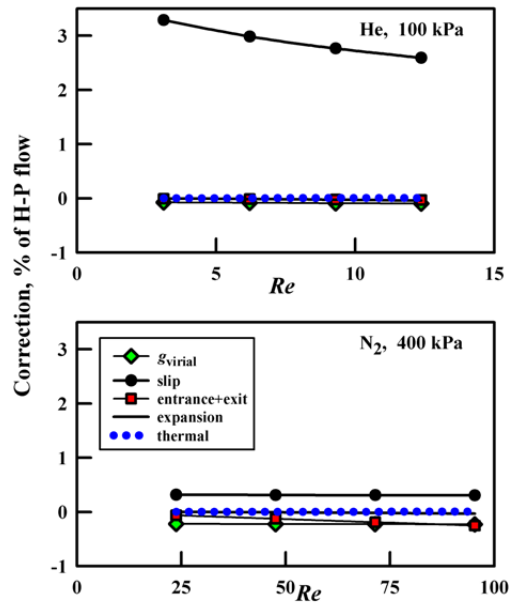


Figure 3. Corrections applied for the annular LFM for a) helium at $P_2 \approx 100$ kPa and b) nitrogen at $P_2 \approx 400$ kPa.

Figure 4 shows the results for the circular segment LFM. The conventional *FC* fit displays errors up to 3.5 % due to its neglect of expansion effects (SF₆) and slip effects (He). Our prior publication [3] contained an incorrect version of Eq. (5). That error did not affect the values for α , β , γ , and δ , but it did affect the values of H and W and the deviation plots. Here, we used the correct version and obtained greatly improved results when estimated K values were used: the model results in Figure 4(B) are within 3 %. However, at $Re > 100$, pressure dependence is observed in the N₂, Ar, and SF₆ data, i.e. higher flow ratios were measured as the pressure was increased from 100 kPa to 400 kPa. The expansion correction term depends on the pressure ratio P_2/P_1 as well as Re . This pressure dependence is significantly reduced by changing K_{exp} from 1 to 0.7, as can be seen by comparing Figures 4(B) and 4(C). Using K values fitted to the N₂ data improves the model results to 1.3 % even for the SF₆ data at Re values more than five times larger than the N₂ data. Figure 4(D) shows that when Eq. (6) is fitted to all gases ($K_{\text{exp}}=0.55$), the results are within 0.5 % of the standard.

For the circular segment LFM, Figure 5 shows the model corrections for SF₆ at two exit pressures, 100 kPa and 400 kPa. The expansion correction is larger at the lower pressure (5 % vs 0.5 %) because, at higher pressures, $P_2 \rightarrow P_1$ for a given flow rate and the $\ln(P_2/P_1)$ dependence of this correction term approaches zero.

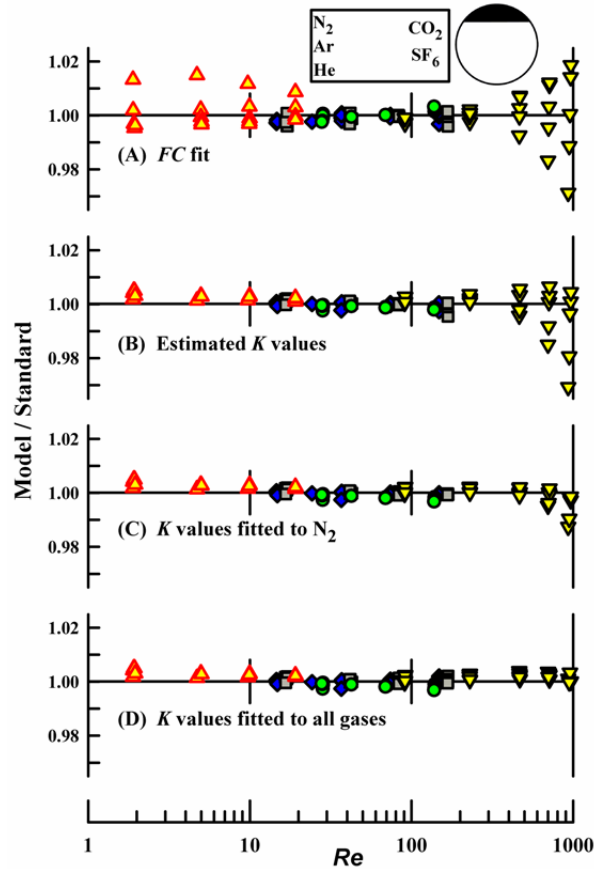


Figure 4. Flow ratio versus Reynolds number for the circular segment LFM.

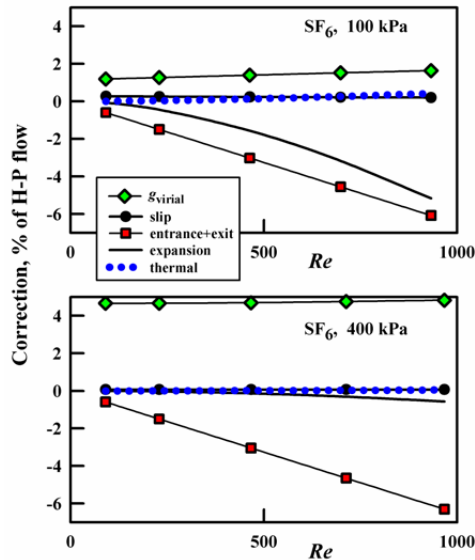


Figure 5. Corrections applied for the circular segment LFM for SF₆ at a) $P_2 \approx 100$ kPa and b) $P_2 \approx 400$ kPa.

Figure 6 shows the results for the circular LFM. The second-order FC fit gives flow ratios within 1 % of the standard because the entrance and exit effects are the dominant corrections

(43 % of H-P flow \dot{m}_0) and depend on Re . All other correction terms are $< 5\%$ of \dot{m}_0 . Figure 6(B) shows that estimated K values give 2 % results. Figure 6(C) shows that fitted K values give improved results for $Re < 500$, but that extrapolation to $Re > 500$ leads to errors up to 7.5 % (beyond the scale of the figure as indicated by the down arrows).

The curvature apparent in these two plots could not be removed by fitting $(K_{ent} + K_{exit})$ or K_{exp} . However, multiplying Eq. (6) by the *ad hoc* function $1 + 1.8 \times 10^{-5} Re + 5.8 \times 10^{-8} Re^2$ did correct the curvature, as shown in 6(D), where all results are within 0.8 % of the standard. We note that the *ad hoc* function of Re is functionally similar to the second-order FC fit, which also fits the experimental data well.

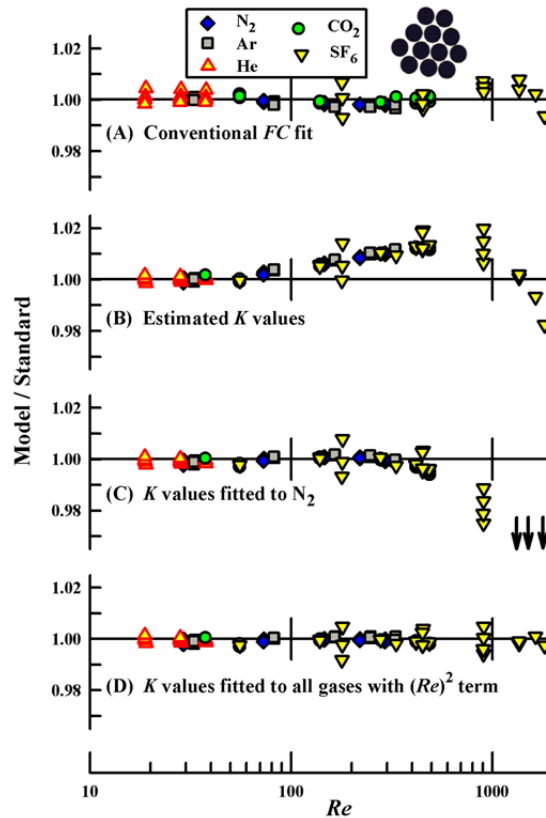


Figure 6. Flow ratio versus Reynolds number for the circular LFM.

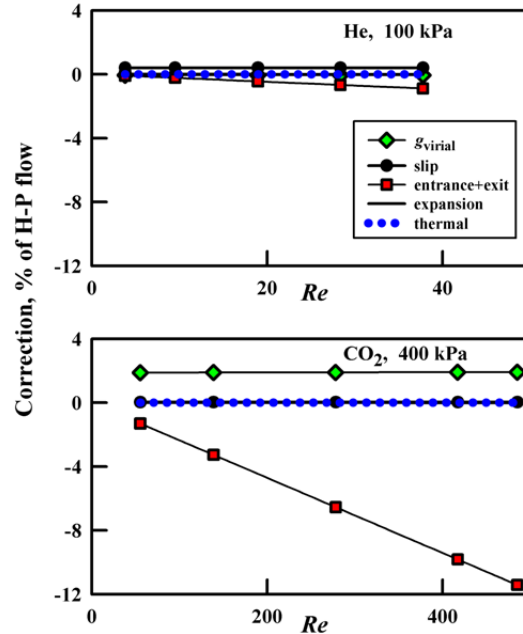


Figure 7. Corrections applied for the circular LFM for a) helium at $P_2 \approx 100$ kPa and b) carbon dioxide at $P_2 \approx 400$ kPa.

Equation (6) is a linear function of Re because the corrections are calculated only to first-order and are assumed to act independently. This linear model is no longer valid when the entrance and exit effects are large. For example, each LFM has an entrance length L_e , over which the uniform entrance profile develops into the invariant quadratic profile assumed by the H-P equation. For the circular LFM, which has the smallest aspect ratio, that length is $L_e = 0.06D_h Re = 0.62L$ at $Re = 1800$ [8]. Thus, only 38 % of the length of the circular LFM contained the fully developed flow assumed by the H-P equation. Another justification for a term proportional to Re^2 is interactions between corrections.

A notable pressure dependence in the SF_6 data remains unexplained. Without the SF_6 pressure dependence and the lowest pressure helium data, the data scatter would be < 0.3 %. We also note that we used the LFM at eight times the maximum Re recommended by the manufacturer.

For the circular LFM, Figure 7 shows that the corrections vary widely with the gas used. For helium at 100 kPa, all the corrections are $< 1\%$, but for CO_2 at 400 kPa, the virial corrections are 2 % and the entrance and exit corrections are as large as 12 %.

5. Summary

Our flow measurements and their interpretation rely on measurements of absolute pressure, differential pressure, temperature, and mass flow, and values of the compressibility, density, and viscosity from the database REFPROP [1]. (REFPROP 9.0. does not contain values for the viscosity of SF_6 ; for that gas, we used the viscosity measured in [15].) The most significant associated uncertainties are for the measurements of differential pressure at 10 % of the LFM full scale flow (0.25 %).

Equation (6) gives a physical model for the laminar flow meter based on the Hagen-Poiseuille equation, generalized for various flow geometries, with corrections for the effects of gas non-ideality, slip, entrance and exit flows, gas expansion through the meter, and heat transfer. For three commercially produced LFMs, the parameters of the LFM model were based on the shape of the LFM cross section, literature values, and calibrations of the LFMs in nitrogen, argon, helium, carbon dioxide, and sulfur hexafluoride for a range of flows (10% to 100 % of full scale flow) and pressures (100 kPa to 400 kPa). The LFM model was evaluated by plotting the ratio of the flow predicted by the model to the flow measured by the reference flow standards with uncertainty $< 0.1\%$.

These measurements demonstrate the significance of the corrections in Eq. (6) for commercial LFMs and explore the limitations of the model. Our helium data demonstrate the significance of the slip correction at atmospheric pressure for the two meters where the mean free path is a significant fraction of the smallest transverse dimension. The large molar mass of sulfur hexafluoride emphasizes the corrections that are related to kinetic energy and thus Re . (Some process gases, e.g. WF_6 , have larger molar masses than SF_6 .) In fact, the maximum value of Re likely exceeded that for the transition from laminar to turbulent flow, which ranges from 200 for short metal tubes to 2300 for long glass tubes [5]. The non-ideal behavior of CO_2 and SF_6 at the higher pressures demonstrates the importance of virial corrections. Our use of pressures between 100 kPa and 400 kPa tested the expansion and virial corrections.

For all three LFMs, Eq. (6) and our flow standards agreed within $< 3\%$ when we used values of K estimated from dimensions as in [3]. When we fitted $(K_{ent} + K_{exit})$ and K_{exp} to nitrogen flow data, the agreement improved to 0.8% for the five gases tested in the range $Re < 500$. When Eq. (6) was extrapolated to $Re = 1800$ using the nitrogen flow parameters, errors as large as 7.5% resulted. Refitting $(K_{ent} + K_{exit})$ and K_{exp} to all five gases reduced the errors for the annular and circular segment to $\leq 0.5\%$. For the circular LFM, we had to multiply Eq. (6) by a second-order function of Re to obtain deviations $\leq 0.8\%$. We speculate that this function accounts for the long entrance length and large end corrections due to the small aspect ratio of this LFM.

The results are instructive to those who use LFMs with multiple gases, and it motivates us to move beyond FC fits. We anticipate that laboratories that calibrate LFMs will design data collection protocols optimized to determine the LFM model parameters, *i.e.* D_h , $K_{ent} + K_{exit}$, and K_{exp} . This protocol could use only one gas if it spanned a wide range of average pressures and flows.

Acknowledgements: We thank Gina Kline for her assistance collecting LFM data, and Casey Rombouts for helpful conversations.

[1] Lemmon EW, McLinden MO and Huber ML, "Refprop: Reference Fluid Thermodynamic and Transport Properties," NIST Standard Reference Database 23, Version 9.0, National Institute of Standards and Technology, Boulder, CO, 2010, <http://www.nist.gov/srd/nist23.cfm>.

[2] Berg RF, Simple Flow Meter and Viscometer of High Accuracy for Gases, *Metrologia*, 42, pp. 11 to 23, 2005. Erratum 43, pp. 183, 2006.

[3] Cobu T, Berg RF, Wright JD, Moldover, MR, Modeling Laminar Flow Meters for process Gases, FLOMEKO Proceedings, Taiwan, 2010.

- [4] Feng CC, Lin WT, and Yang CT, Laminar Flow Element Type Flow Meter with Straight Glass Capillary, FLOMEKO Proceedings, Taiwan, 2010.
- [5] Kawata M, Murase K, Nagashima A, and Yoshida K, Capillary Viscometers, Measurement of the Transport Properties of Fluids, Wakeham WA, *et al.* editors, Oxford: Blackwell, 1991.
- [6] Todd DA, Laminar Flow Elements in Flow Measurement: Practical Guides for Measurement and Control, 2nd edition, Spitzer DW editor, The Instrumentation, Systems, and Automation Society, Research Triangle Park, North Carolina, pp. 205 to 239, 2001.
- [7] Wright JD, The Long Term Calibration Stability of Critical Flow Nozzles and Laminar Flow Meters, National Conference of Standards Laboratories Conference Proceedings, Albuquerque, New Mexico, pp. 443 to 462, 1998.
- [8] Shah RK and London AL, Laminar Flow Forced Convection in Ducts, in Advances in Heat Transfer, Irvine TF and Hartnett JP editors, Academic Press, 1978,
- [9] White FM, Viscous Fluid Flow, 2nd edition, McGraw Hill, 1991.
- [10] Berg RF and Tison SA, Laminar Flow of Four Gases through a Helical Rectangular Duct, AIChE Journal 47, 2, pp. 263 to 270, 2001.
- [11] van den Berg HR, ten Seldam CA, and van der Gulik PS, Compressible Laminar Flow in a Capillary, J. Fluid Mech., 246, pp. 1 to 20, 1993.
- [12] van den Berg HR, ten Seldam CA, and van der Gulik PS, Thermal Effects in Compressible Viscous Flow in a Capillary, Int. J. Thermophys., 14, pp. 865, 1993.
- [13] Wright JD and Johnson AN, NIST Lowers Gas Flow Uncertainties to 0.025 % or Less, NCSL International Measure, 5, pp. 30 to 39, March, 2010.
- [14] Bair M and Rombouts C, Typical Measurement Uncertainty in Gas Flow Measured by GFS2102 Gravimetric Flow Standard, Technical Note 6050TN09, DH Instruments, May 31, 2006.
- [15] Strehlow T and Vogel E, Temperature Dependence and Initial Density Dependence of the Viscosity of Sulfur Hexafluoride, Physica A, 161,101, 1989.